Aerosol and Air Quality Research, 18: 1068–1079, 2018

ISSN: 1680-8584 print / 2071-1409 online
doi: 10.4209/aaqr.2016.06.0282

Impact of Aerosol Direct Effect on Wintertime $PM_{2.5}$ Simulated by an Online Coupled Meteorology-Air Quality Model over East Asia

Ami Sekiguchi*, Hikari Shimadera, Akira Kondo

Graduate School of Engineering, Osaka University, Suita, Osaka 565-0871, Japan

ABSTRACT

This study aims to evaluate the impacts of the aerosol direct effect on simulated concentrations of fine particulate matter ($PM_{2.5}$) over East Asia, which is controlled by heavy local air pollution and long-range transport. The online coupled Weather Research and Forecasting-Community Multiscale Air Quality (WRF-CMAQ) modeling system was applied to one-way and two-way simulations (without and with the aerosol direct effect) of a period from January till March of 2014. The differences between the two simulations showed that there were particularly large impacts of the aerosol direct effect on the eastern Asian continent with high aerosol loading. The temporal mean contributions of the direct effect averaged over the regions from Northeast to Central China were a 15% decrease in the surface shortwave radiation, a 9.0% decrease in the planetary boundary layer (PBL) height, and an 8.6% increase in the ground-level $PM_{2.5}$ concentration. In addition, there were negative contributions of the direct effect to the $PM_{2.5}$ concentration over the ocean from the Sea of Japan to the East China Sea (a 1.0% decrease on average throughout the period). The $PM_{2.5}$ decrease over the ocean was likely attributable to a reduction in the secondary $PM_{2.5}$ outflow from the continent to the downwind region, which was caused by the increased dry deposition of $PM_{2.5}$ precursors from the increased ground-level concentrations within a more stable PBL over the continent. Overall, the substantial decrease in the surface shortwave radiation due to the aerosol direct effect led to enhanced atmospheric stability and therefore increased the ground-level $PM_{2.5}$ in the heavily polluted region.

Keywords: Online coupled WRF-CMAQ model; Shortwave radiative feedback; Atmospheric stability; Fine particulate matter.

INTRODUCTION

Aerosol particles can be generated naturally or anthropogenically from various sources including direct emissions into the atmosphere (e.g., biomass burning, dust and sea salt) and secondary formations through gas-to-particle conversion (e.g., oxidations of sulfur dioxide, nitrogen oxides and volatile organic compounds). The presence of aerosol particles affects the solar radiation by scattering and absorption in the atmosphere, which is called the aerosol direct effect. The direct effect can cause changes in photolysis rates for photochemistry and surface temperature that affects atmosphere stability controlling vertical dispersion of air pollutants (Wong *et al.*, 2012; Xing *et al.*, 2015).

In Asia, the rapid growth in economic activities and energy consumption in recent decades has caused tremendous increases in anthropogenic emissions of air pollutions (Ohara *et al.*, 2007; Kurokawa *et al.*, 2013). As a result, this region has faced severe air pollution by aerosol particles including particulate matter with an aerodynamic diameter of 2.5 μm or less ($PM_{2.5}$), particularly in winter (e.g., Yu *et al.*, 2014b; Jiang *et al.*, 2015; Yan *et al.*, 2015; Cheng *et al.*, 2016). A large number of numerical studies have focused on severe local air pollution in the region, such as a severe haze episode over the North China Plain in January 2013 (e.g., Shimadera *et al.*, 2014; Uno *et al.*, 2014; Wang *et al.*, 2014; Zheng *et al.*, 2015). In addition, since air pollutants from the Asian Continent are efficiently transported to the Pacific region, long-range transport of air pollutants from the continent has been a field of scientific interests (e.g., Shimadera *et al.*, 2013; Chen *et al.*, 2014; Itahashi *et al.*, 2016).

Although air quality modeling studies have generally used offline one-way models that do not consider feedbacks from chemistry to meteorology (e.g., Shimadera *et al.*, 2013; Chen *et al.*, 2014; Shimadera *et al.*, 2014; Tan *et al.*, 2015; Zheng *et al.*, 2015; Itahashi *et al.*, 2016), there are increasing applications of online coupled models with the feedbacks (e.g., Yu *et al.*, 2014a; Wang *et al.*, 2014; Hogrefe *et al.*, 2015; Kong *et al.*, 2015). In Asia with substantial aerosol loading, aerosol particles are likely to have important influence on meteorology, and in turn, on the atmospheric

*Corresponding author.
Tel.: +81-6-6879-7668; Fax: +81-6-6879-7668
E-mail address: sekiguchi@ea.see.eng.osaka-u.ac.jp

chemical transport. However, almost all of previous studies in Asia using online coupled models have focused only on heavy local pollution in China (e.g., Wang *et al.*, 2014), thus, the impacts of the feedback on air quality simulations in Asia are far from being well understood.

In this study, an online coupled meteorology-air quality modeling system was applied to wintertime $PM_{2.5}$ simulations over East Asia in order to evaluate the impacts of the aerosol direct effect on the surface shortwave radiation, atmospheric stability and dispersion of $PM_{2.5}$. This study focused on the impacts of the aerosol direct effect to the simulations of not only heavy local pollution, but also long-range atmospheric transport.

METHODOLOGY

Online Coupled WRF-CMAQ Modeling System

The online coupled meteorology and air quality modeling system used in the present study consists of three components: the Weather Research and Forecasting model (WRF) (Skamarock *et al.*, 2009) version 3.4 developed by the United States National Center for Atmospheric Research (NCAR), the Community Multiscale Air Quality model (CMAQ) (Byun and Ching, 1999) version 5.0.2 developed by the U.S. Environmental Protection Agency (the U.S. EPA) and an inter-model coupler to ensure data exchange between WRF and CMAQ (Wong *et al.*, 2012). In this online coupled system, aerosol concentration, composition and size distribution simulated in CMAQ are used to estimate the optical properties of aerosols, which are then used in calculations of the shortwave radiation in WRF (i.e., the aerosol direct effect on the shortwave radiation). More detailed information about the online coupled WRF-CMAQ system can be found in Wong *et al.* (2012).

Simulation Design

Fig. 1 shows the modeling domain for the WRF-CMAQ simulations, which covers a wide area of East Asia including China and Japan, with the location of observation sites (Table 1) for the model evaluation and a line indicating the target area for an analysis of eastward $PM_{2.5}$ flux (Subsection 3.2.2). The horizontal resolution is 45 km × 45 km and the number of grid cells is 140 × 120 for the WRF simulations and 130 × 110 for the CMAQ simulations, respectively. The vertical layers consist of 30 sigma-pressure layers from the surface to 100 hPa. The top height of the first layer is approximately 50 m and there are 10 layers from the surface to about 2000 m. The model simulation period is from January to March 2014 with an initial spin-up period of 22–31 December 2013. In order to evaluate the impacts of the aerosol direct effect on $PM_{2.5}$ simulations, the WRF-CMAQ simulations were conducted for the following two cases: the one-way case without the feedback from chemistry to meteorology and the two-way case with the feedback. The contribution of the aerosol direct effect was calculated as the difference of the two cases (two-way–one-way), and the contribution percentage was calculated as the ratio of this difference to the one-way simulation. Note that because photolysis rates were calculated with an in-line module of CMAQ (Binkowski *et al.*, 2007), which takes account of time-dependent gases and aerosol particles in the atmosphere, both in the one-way and two-way simulations, the contribution of the direct effect estimated in this study was mainly due to changes in the surface temperature and atmosphere stability.

Model Setup

For the WRF simulations, initial and boundary conditions were derived from a combination of the real time, global

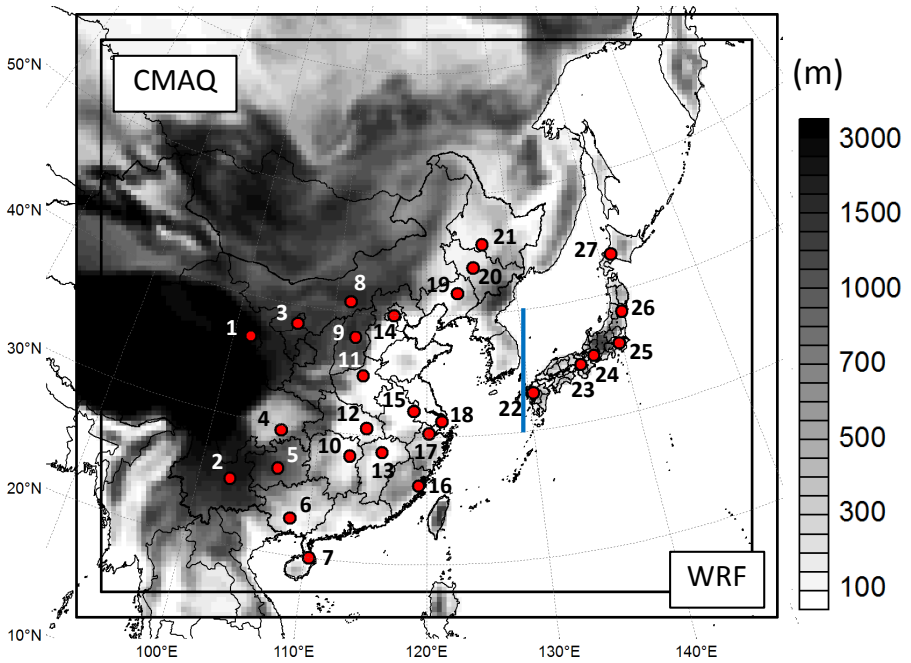

Fig. 1. Modeling domain and locations of observation sites. Site names corresponding to site numbers are shown in Table 1. A line indicating the target area for an analysis of eastward $PM_{2.5}$ flux is provided.

Table 1. Observation sites for the model evaluation with site numbers assigned in the order from the west to the east.

China			
1	Xining	12	Wuhan
2	Kunming	13	Nanchang
3	Yinchuan	14	Beijing
4	Chongqing	15	Nanjing
5	Guiyang	16	Fuzhou
6	Nanning	17	Hangzhou
7	Haikou	18	Shanghai
8	Hohhot	19	Shenyang
9	Taiyuan	20	Changchun
10	Changsha	21	Harbin
11	Zhengzhou		
Japan			
22	Fukuoka	25	Tokyo
23	Osaka	26	Sendai
24	Nagoya	27	Sapporo

analysis, high-resolution sea surface temperature (RTG_SST_HR) data by the U.S. National Centers for Environmental Prediction (NCEP), the mesoscale model grid point value (MSM-GPV) data by the Japan Meteorological Agency (JMA) and the final analysis (FNL) data by NCEP. The physics options of WRF included the Morrison double-moment scheme for the microphysics parameterization (Morrison *et al.*, 2009), the Kain-Fritsch scheme for the cumulus (Kain, 2004), the Pleim-Xiu land surface model for the land surface (Xiu and Pleim, 2001), the asymmetric convection model version 2 (ACM2) scheme for the planetary boundary layer (PBL) (Pleim, 2007), the Pleim-Xiu scheme for the surface layer (Pleim, 2006) and the rapid radiative transfer model for global climate models (RRTMG) scheme for the longwave and shortwave radiation (Iacono, 2008). For better representation of the realistic atmosphere, grid nudging was applied to temperature, humidity and horizontal wind components in the entire simulation period with a nudging coefficient of 3×10^{-4} s^{-1}. However, since the grid nudging could dampen the aerosol direct effect in the simulations (e.g., Hogrefe *et al.*, 2015), it was used only above the PBL in order to properly evaluate the impacts of the aerosol direct effect at least within PBL.

For the CMAQ simulations, boundary concentrations were derived from the Model Ozone and Related Chemical Tracers version 4 (MOZART-4) (Emmons *et al.*, 2010) driven by meteorological fields from the Goddard Earth Observing System version 5 (GEOS-5) (Rienecker *et al.*, 2008). The chemistry options of CMAQ included the Carbon Bond mechanism developed in 2005 (CB05) (Whitten *et al.*, 2010) for the gas-phase chemistry, the sixth generation CMAQ aerosol module (AERO6) for the aerosol process, and the on-line photolysis rate module with the radiative impacts of simulated aerosol loading. Anthropogenic and natural emission data were obtained by the same method as used by Shimadera *et al.* (2016): Anthropogenic emissions in Japan were derived from the Japan Auto-Oil Program (JATOP) Emission Inventory-Data Base (JEI-DB) developed by Japan Petroleum Energy Center (JPEC, 2012) for vehicles, an emission inventory developed by the Ocean Policy Research Foundation (OPRF, 2012) for ships, and an emissions inventory called EAGrid2010-JAPAN (Fukui *et al.*, 2014) for the other sectors. Anthropogenic emissions except Japan were mainly derived from an emission inventory to support the Intercontinental Chemical Transport Experiment phase B (INTEX-B) (Zhang *et al.*, 2009) version 1.2. Biogenic emissions were estimated with the Model of Emissions of Gases and Aerosols from Nature (MEGAN) (Guenther *et al.*, 2006) version 2.04. Daily emissions from open biomass burning were derived from the Fire INventory from NCAR (FINN) (Wiedinmyer *et al.*, 2011) version 1.5. Volcanic SO_2 emissions were derived from the Aerosol Comparisons between Observations and Models (AeroCom) data (Diehl *et al.*, 2012). Fig. 2 shows a spatial distribution of mean primary $PM_{2.5}$ emissions. There are a large amount of anthropogenic emissions in China, particularly eastern urban area such as Beijing (site 14 in Fig. 1) and its surrounding areas, and biomass burning emissions in Southeast Asia.

Observational Data

The WRF-CMAQ performance was evaluated using observation data from 27 sites (21 sites in China and 6 sites in Japan) located in major cities (Fig. 1 and Table 1). Observed data of meteorological variables such as temperature, humidity and wind speed, and $PM_{2.5}$ concentration are available at these sites. These meteorological variables at 19 sites (except Xining and Wuhan because of lack of data) in China were obtained from the atmospheric sounding data at 0:00 and 12:00 UTC collected by University of Wyoming (http://weather.uwyo.edu/upperair/sounding.html). Daily $PM_{2.5}$ concentrations at the 21 sites in China were obtained from a historical data archive (http://www.aqistudy.cn/historydata/index.php). Hourly meteorological variables at meteorological observatories in Japan were extracted from monthly datasets by Japan Meteorological Business Support Center (http://www.jmbsc.or.jp/hp/offline/cd0061.html). Hourly $PM_{2.5}$ concentrations observed at ambient air pollution monitoring stations in Japan were extracted from the Environmental Numerical Databases by the National Institute for Environmental Studies of Japan (https://www.nies.go.jp/igreen).

Statistical Analysis

The WRF-CMAQ performance for meteorological simulations was evaluated using the following statistical parameters: the mean, the mean bias (MB), the Pearson's correlation coefficient (r), the mean absolute error (MAE), the root mean square error (RMSE) and the index of agreement (IA). For the evaluation of the meteorological model performance, Emery *et al.* (2001) proposed the following benchmarks: MB $\leq \pm$ 0.5°C, MAE $\leq$ 2°C and IA $\geq$ 0.8 for temperature, MB $\leq \pm$ 1 g kg^{-1}, MAE $\leq$ 2 g kg^{-1} and IA $\geq$ 0.6 for humidity, and MB $\leq \pm$ 0.5 m s^{-1}, RMSE $\leq$ 2 m s^{-1} and IA $\geq$ 0.6 for wind speed. These standards were used to evaluate the meteorological performance of the WRF-CMAQ modeling system. In addition, the normalized mean bias (NMB) and the mean normalized bias (MNB) were

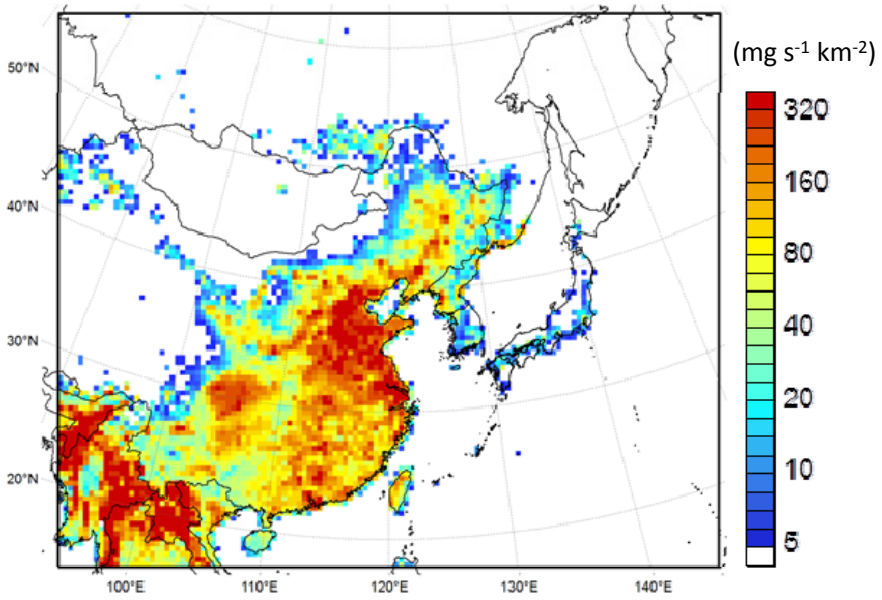

Fig. 2. Spatial distributions of mean primary $PM_{2.5}$ emissions.

used for the evaluation of the WRF-CMAQ performance for $PM_{2.5}$ simulations. The definitions of the statistical parameters are as follows:

$$\mathrm{MB} = \bar{M} - \bar{O} \tag{1}$$

$$r = \frac{\sum_{i=1}^{N}\left(M_i - \bar{M}\right)\left(O_i - \bar{O}\right)}{\left\{\sum_{i=1}^{N}\left(M_i - \bar{M}\right)^2 \sum_{i=1}^{N}\left(O_i - \bar{O}\right)^2\right\}^{\frac{1}{2}}} \tag{2}$$

$$\mathrm{MAE} = \frac{1}{N}\sum_{i=1}^{N}\left|M_i - O_i\right| \tag{3}$$

$$\mathrm{RMSE} = \left[\frac{1}{N}\sum_{i=1}^{N}\left(M_i - O_i\right)^2\right]^{\frac{1}{2}} \tag{4}$$

$$\mathrm{IA} = 1 - \frac{\sum_{i=1}^{N}\left(M_i - O_i\right)^2}{\sum_{i=1}^{N}\left(\left|M_i - O\right| + \left|O_i - \bar{O}\right|\right)^2} \tag{5}$$

$$\mathrm{NMB} = \frac{\bar{M}}{\bar{O}} - 1 \tag{6}$$

$$\mathrm{MNB} = \frac{1}{N}\sum_{i=1}^{N}\left(\frac{M_i}{O_i} - 1\right) \tag{7}$$

where $\bar{M}$ and $\bar{O}$ are respectively mean model-predicted and observed values, M_i and O_i are respectively model-predicted and observed values, and N is the number of samples.

RESULTS AND DISCUSSION

Model Performance

Table 2 shows statistical comparisons between the simulated and observed daily average ground-level air temperature, humidity and wind speed for the 19 sites in China, the 6 sites in Japan, Beijing (site 14 in Fig. 1) and Osaka (site 23 in Fig. 1). Note that the statistical comparisons in China were obtained from the observed and simulated values data at 0:00 and 12:00 UTC (8:00 and 20:00 local time). For temperature, the one-way and two-way simulations by the WRF-CMAQ modeling system satisfied the Emery's benchmark for MB at 3 and 4 sites out of the 19 sites in China, 1 and 1 site out of the 6 sites in Japan, for MAE at 9 and 9 sites in China, 3 and 3 sites in Japan, and for IA at 18 and 18 sites in China, 6 and 6 sites in Japan, respectively. For humidity, the simulations met all the benchmarks at all the sites except Chongqing. Although temperature was generally underestimated, the good correlations for temperature and humidity both in China and Japan ($r > 0.9$) indicate that the model successfully simulated their spatial and temporal variations. For wind speed, the one-way and two-way simulations satisfied the benchmark for MB at 4 and 4 sites out of the 19 sites in China, 1 and 2 sites out of the 6 sites in Japan, for RMSE at 16 and 16 sites in China, 5 and 5 sites in Japan, and for IA at 10 and 10 sites in China, 4 and 4 sites in Japan, respectively. Although the model performance for wind speed was generally inferior to those for temperature and humidity according to IA, a similar trend is also found in previous studies (e.g., Shimadera *et al.*, 2013). In addition, WRF simulations with finer horizontal resolutions (several kilometers) in Japan (e.g., Shimadera *et al.*, 2013) have shown better performance compared to this study, indicating that the direct comparisons of the simulations using the coarse horizontal resolution (45 km × 45 km) with the pointwise observations may be partly responsible for the discrepancies between the observations and simulations. According to the

Table 2. Statistical evaluation of meteorological simulations.

	n	Mean (Obs)		Mean (Model)	MB	*r*	MAE	RMSE	IA
Temperature		(°C)		(°C)	(°C)		(°C)	(°C)	
China	1690	4.7	two-way	3.0	–1.7	0.97	2.5	3.3	0.97
			one-way	3.3	–1.4	0.97	2.4	3.3	0.97
Japan	540	5.1	two-way	4.0	–1.2	0.95	1.8	2.1	0.96
			one-way	4.1	–1.1	0.95	1.7	2.0	0.96
Beijing	89	2.3	two-way	0.4	–1.8	0.98	1.9	2.2	0.97
			one-way	0.9	–1.4	0.97	1.6	2.0	0.97
Osaka	90	7.2	two-way	4.9	–2.4	0.96	2.4	2.5	0.88
			one-way	5.0	–2.3	0.96	2.3	2.4	0.89
Humidity		(g kg^{-1})		(g kg^{-1})	(g kg^{-1})		(g kg^{-1})	(g kg^{-1})	
China	1690	4.5	two-way	4.4	–0.1	0.97	0.5	0.9	0.98
			one-way	4.4	–0.1	0.97	0.6	0.9	0.98
Japan	540	3.5	two-way	3.9	0.4	0.96	0.5	0.6	0.96
			one-way	3.9	0.4	0.95	0.5	0.6	0.96
Beijing	89	2.2	two-way	2.1	0.0	0.96	0.3	0.4	0.98
			one-way	2.1	–0.1	0.96	0.3	0.4	0.98
Osaka	90	4.0	two-way	4.2	0.2	0.97	0.3	0.4	0.98
			one-way	4.2	0.2	0.97	0.3	0.4	0.98
Wind speed		(m s^{-1})		(m s^{-1})	(m s^{-1})		(m s^{-1})	(m s^{-1})	
China	1690	2.4	two-way	3.3	0.9	0.46	1.4	1.8	0.61
			one-way	3.4	1.0	0.46	1.4	1.8	0.61
Japan	540	3.2	two-way	4.6	1.4	0.62	1.6	2.3	0.63
			one-way	4.6	1.4	0.62	1.6	2.3	0.63
Beijing	89	2.0	two-way	2.8	0.8	0.47	1.0	1.2	0.57
			one-way	2.8	0.8	0.44	1.0	1.2	0.54
Osaka	90	2.3	two-way	4.0	1.6	0.74	1.6	1.8	0.48
			one-way	4.0	1.7	0.74	1.7	1.9	0.48

Note: *n*: sample number, MB: mean bias, *r*: Pearson's correlation coefficient, MAE: mean absolute error, RMSE: root mean square error and IA: index of agreement.

statistical evaluation, the overall performances for simulating the meteorological variables in the one-way and two-way cases were quite similar to each other. Meanwhile, the ground-level temperature tended to be lower in the two-way simulation than the one-way simulation, which was likely caused by the reduction of surface shortwave radiation by aerosol scattering.

Table 3 shows statistical comparisons between the simulated and observed daily $PM_{2.5}$ concentrations for the 21 sites in China and the 6 sites in Japan, Beijing and Osaka, and Fig. 3 shows time-series of daily $PM_{2.5}$ concentrations at Beijing and Osaka, respectively. Both the one-way and the two-way simulations well captured day-to-day variations in $PM_{2.5}$ concentration including the occurrence of several high peaks at Beijing and Osaka. The model performances in the two cases were almost identical in Japan. The model performance in the two-way simulation with the aerosol feedback was slightly better at Beijing with higher $PM_{2.5}$ concentrations especially in heavy pollution events. For the 21 sites in China, although there were larger overestimates in the two-way simulation according to MB, NMB and MNB, the model performances in the two cases were similar to each other according to IA. In addition to considering the aerosol direct effect, it is also important to improve other model processes including emission, transport, reaction and deposition because their mutual interactions determine the overall model performance.

Impacts of Aerosol Direct Effect

Impacts on $PM_{2.5}$ at Observation Sites

Fig. 4 shows spatial distributions of mean ground-level concentrations of total, primary and secondary (= sulfate + nitrate + ammonium + secondary organic aerosol) $PM_{2.5}$ for the two-way simulation during the simulation period over the whole domain. The simulated mean $PM_{2.5}$ concentration was much higher over the Asian Continent, especially the regions from Northeast to Central China (Liaoning, Jilin and Heilongjiang in Northeast China; Beijing, Tianjin, Hebei, Shanxi and Inner Mongolia in North China, Shanghai, Jiangsu, Zhejiang, Anhui, Fujian, Jiangxi and Shandong in East China; Henan, Hubei and Hunan in Central China) in which the spatial mean and maximum values in the two-way simulation were respectively about 65 and 180 μg m^{-3}. There was a decreasing trend in the $PM_{2.5}$ concentration from the continent to the Pacific Ocean. This spatial gradient indicates a large contribution of long-range transport of $PM_{2.5}$ from the continent to the downwind area (Shimadera *et al.*, 2016). Except Southeast Asia with substantial biomass burning emissions, the secondary $PM_{2.5}$ concentration was generally higher and more widely distributed compared to the primary $PM_{2.5}$, indicating that the secondary $PM_{2.5}$ mainly contributed to the total concentration of the ground-level

Table 3. Statistical evaluation of $PM_{2.5}$ simulations.

	n	Mean (Obs)		Mean (Model)	MB	NMB	MNB	*r*	MAE	RMSE	IA
***PM*$_{2.5}$**		(μg m^{-3})		(μg m^{-3})	(μg m^{-3})	(%)	(%)		(μg m^{-3})	(μg m^{-3})	
China	1890	76.9	two-way	90.4	13.4	17	32	0.69	35.4	50.7	0.80
			one-way	84.8	7.9	10	26	0.68	32.3	45.7	0.81
Japan	533	16.9	two-way	13.9	–3.0	–18	–15	0.80	5.7	8.5	0.88
			one-way	13.9	–3.1	–18	–15	0.80	5.7	8.5	0.88
Beijing	90	110.7	two-way	113.3	2.6	2	28	0.86	32.4	45.5	0.93
			one-way	103.0	–7.8	–7	21	0.85	32.7	48.0	0.90
Osaka	88	20.4	two-way	15.4	–5.0	–24	–27	0.86	6.8	8.7	0.89
			one-way	15.4	–5.0	–25	–28	0.85	6.8	8.8	0.89

Note: *n*: sample number, MB: mean bias, NMB: normalized mean bias, MNB: mean normalized bias, *r*: Pearson's correlation coefficient, MAE: mean absolute error, RMSE: root mean square error and IA: index of agreement.

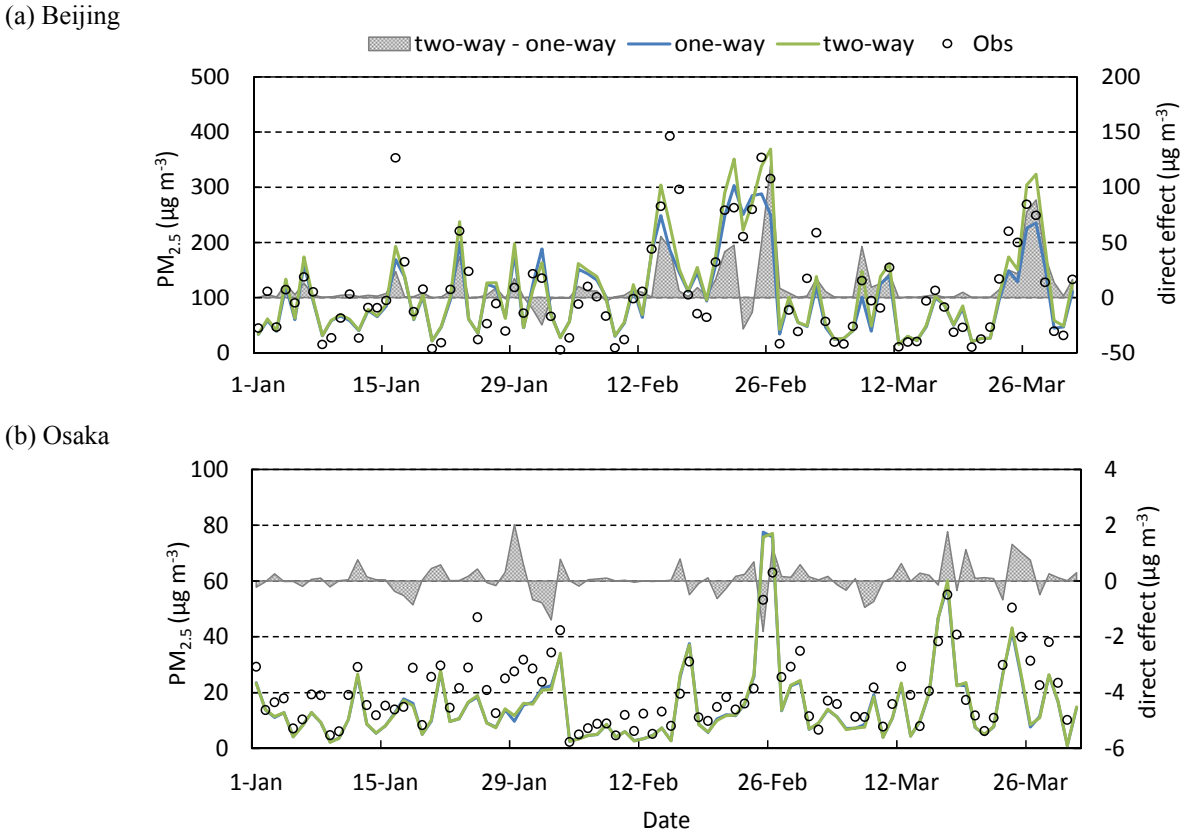

Fig. 3. Time series of observed and simulated ground–level daily $PM_{2.5}$ concentrations at (a) Beijing (site 14 in Fig. 1) and (b) Osaka (site 23 in Fig. 1) with the corresponding contribution of the aerosol direct effect (two-way–one-way) from January to March 2014.

$PM_{2.5}$, and therefore, the long-range transport of $PM_{2.5}$.

Fig. 5 shows comparisons of the mean ground-level $PM_{2.5}$ concentrations between the results of the one-way and the two-way simulations at the 27 sites along with their observations. At the sites in China, the simulated mean $PM_{2.5}$ concentrations in the two-way case ranged from about 15 to 190 μg m^{-3}, while the values were much lower with ranging from about 8 to 20 μg m^{-3} in Japan. The two-way simulation showed higher ground-level $PM_{2.5}$ concentrations than the one-way simulation at 25 sites out of the 27 sites. Moreover, there were larger differences between the one-way and the two-way simulations in areas with severe air pollution, indicating larger impacts of the aerosol direct effect on $PM_{2.5}$ simulations in polluted areas. As shown in Fig. 3, the temporal variation in the contribution of the aerosol direct effect to the ground-level $PM_{2.5}$ concentration at Osaka was quite different from that at Beijing. The large positive contribution dominated at Beijing (Fig. 3(a)) particularly on heavy pollution days. However, the negative contribution was comparable with the positive contribution at Osaka

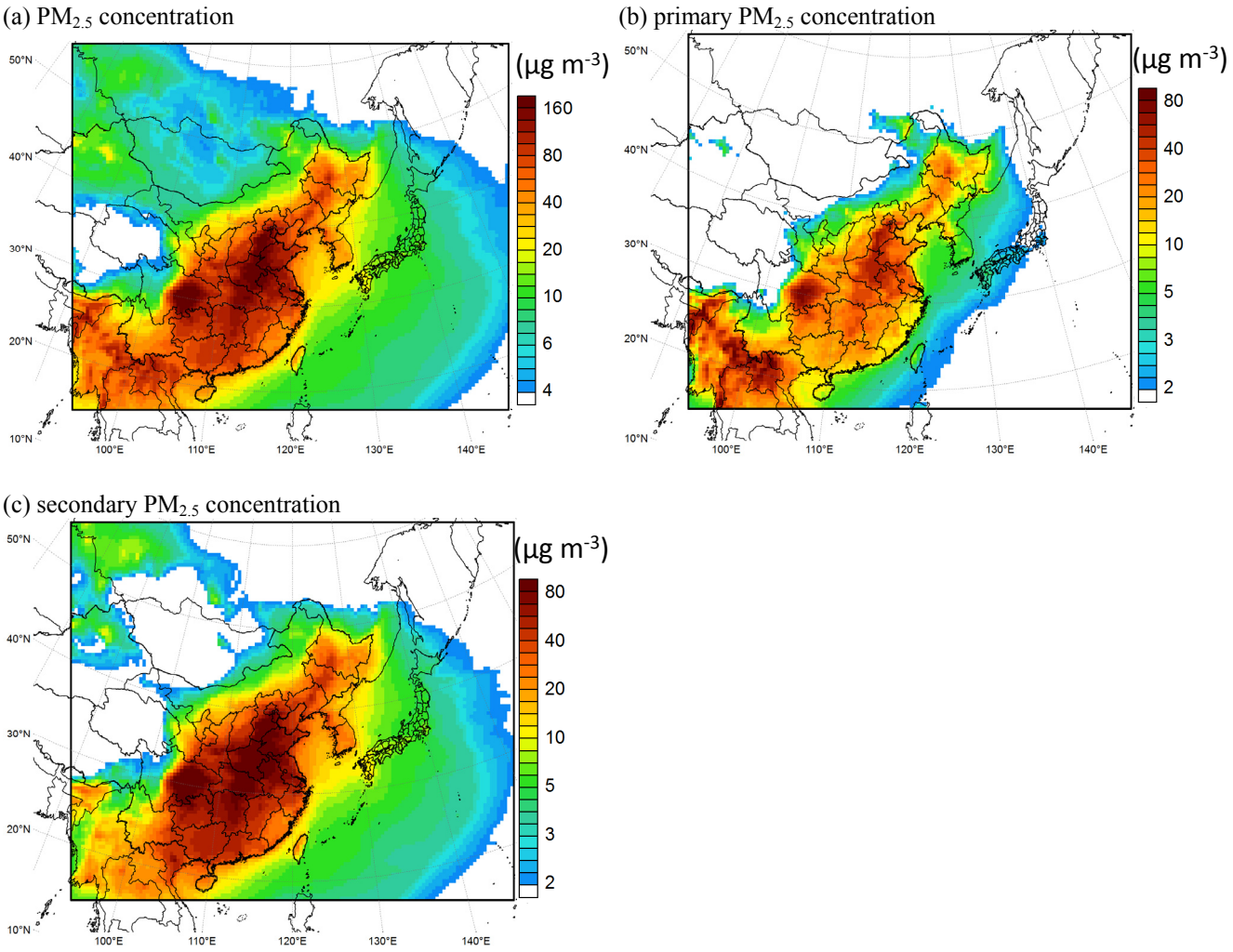

Fig. 4. Spatial distributions of simulated mean ground-level concentrations of (a) total, (b) primary and (c) secondary $PM_{2.5}$ in the two-way case.

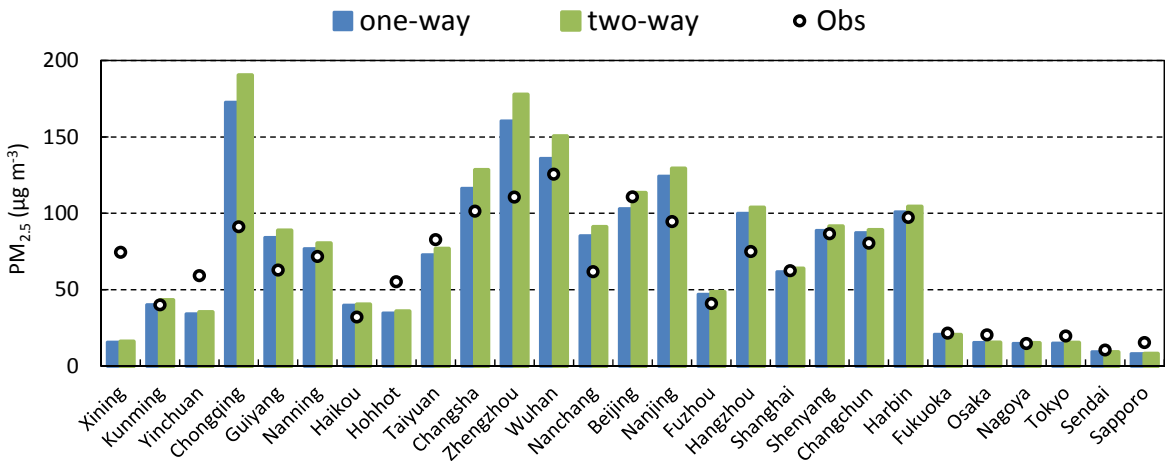

Fig. 5. Comparison of observed and simulated $PM_{2.5}$ concentrations at the 27 observation sites arranged in the order from the west to the east.

(Fig. 3(b)), where both local pollution and long-range transport controlled the $PM_{2.5}$ concentration (Shimadera *et al.*, 2016). Because the $PM_{2.5}$ concentration in heavily polluted areas tended to be overestimated in the two-way case, the contribution of the aerosol direct effect may be somewhat overestimated in this study.

Impacts on Shortwave Radiation, PBL Height and $PM_{2.5}$ Concentration

Fig. 6 shows spatial distributions of mean contribution percentage of the aerosol direct effect to the surface shortwave radiation, PBL height and ground-level concentrations of total, primary and secondary $PM_{2.5}$ in the entire simulation period. The aerosol direct effect decreased the surface shortwave radiation over the simulation domain,

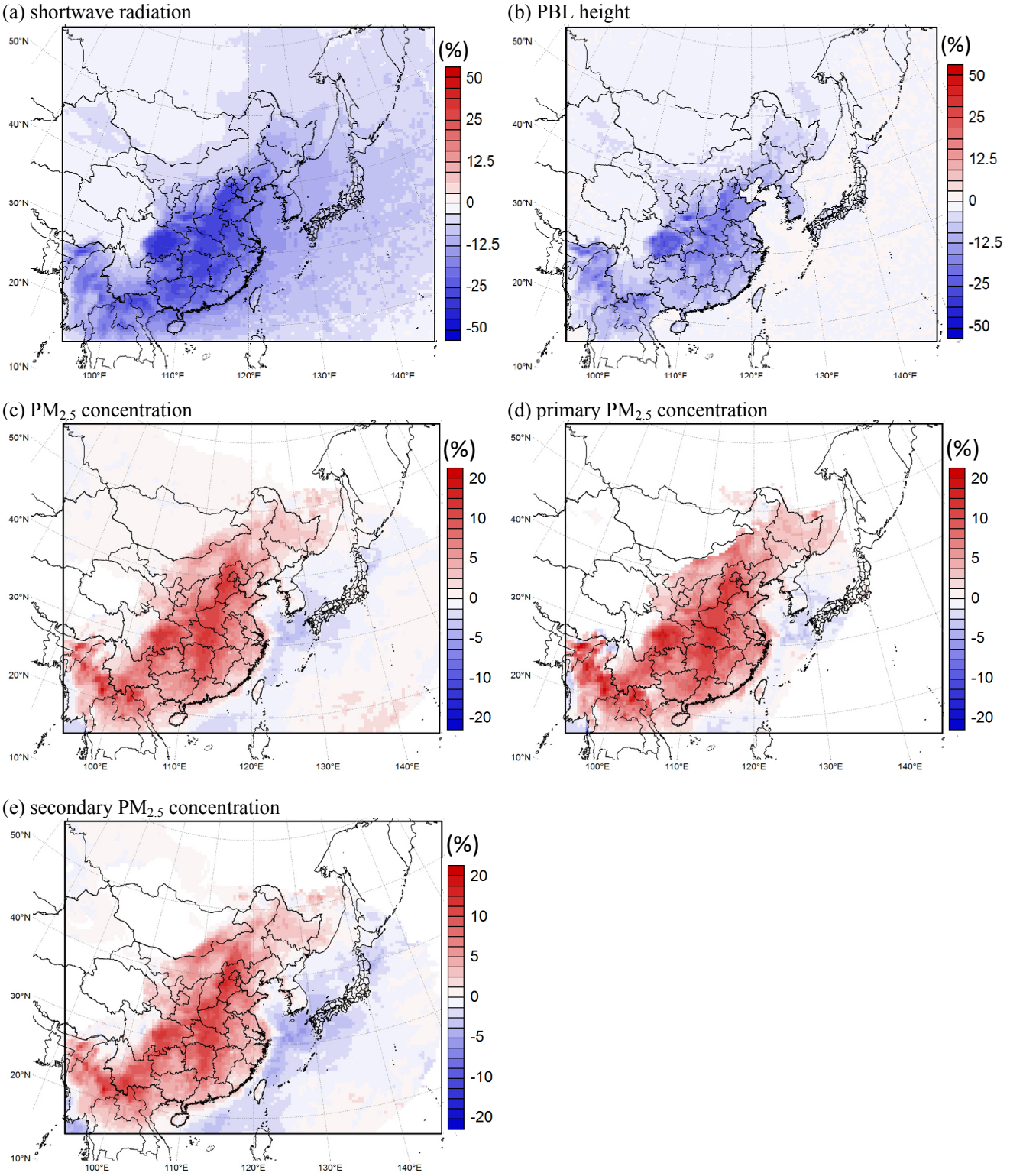

Fig. 6. Spatial distributions of contribution percentage of the aerosol direct effect for (a) surface shortwave radiation, (b) PBL height, and ground-level concentrations of (c) total, (d) primary and (e) secondary $PM_{2.5}$. The contribution percentage for total, primary and secondary $PM_{2.5}$ are shown in grid cells with their concentrations higher than 4, 2 and 2 μg m^{-3}, respectively.

particularly in areas with severe $PM_{2.5}$ pollution (Fig. 4). While the aerosol direct effect reduced PBL height in land areas, there was no clear impact on PBL height over the ocean. This is probably because WRF calculates the surface temperature using the shortwave radiation in land areas, but uses external SST data over the ocean. On the other hand, for the ground-level $PM_{2.5}$ concentration, there were positive contributions of the aerosol direct effect over the eastern region of the Asian Continent and negative contributions over the ocean including the Sea of Japan and the East China Sea. For the shortwave radiation and PBL height, the spatial mean contributions of the aerosol direct effect averaged over the simulation period were about 15% and 9.0% decreases over the regions from Northeast to Central China, and the spatially largest contributions were about 40% and 30% decreases, respectively. For the $PM_{2.5}$ concentration, the spatial mean contributions were 8.6% increase over the regions from Northeast to Central China and 1.0% decrease over the ocean from the Sea of Japan to the East China Sea, and the spatially largest contributions were 20% increase over China and 4.1% decrease over the ocean, respectively. Compared to the primary $PM_{2.5}$, negative contributions of the direct effect to the ground-level secondary $PM_{2.5}$ concentration were larger and more widely distributed over the ocean. The spatial mean contributions of the aerosol direct effect over the ocean from the Sea of Japan to the East China Sea were respectively 0.0% and 2.0% decreases for the primary and secondary $PM_{2.5}$, and the spatially largest negative contributions were respectively 3.2% and 5.9% decreases for the primary and secondary $PM_{2.5}$.

The impacts of the direct effect on $PM_{2.5}$ precursors were evaluated in order to investigate the cause of the larger negative contributions in the secondary $PM_{2.5}$ over the ocean. It was found that dry deposition of $PM_{2.5}$ precursors over the continent was larger because of larger ground-level concentrations under more stable atmospheric condition in the two-way case. The positive contributions of the direct effect to the total dry deposition of SO_2, NH_3 and NO were respectively 2.0, 3.5 and 5.5% increases over the continent in the simulation period. The increase in dry deposition of the $PM_{2.5}$ precursors resulted in a decrease in the total production of secondary $PM_{2.5}$ over the continent. As mentioned in Subsection 3.2.1, the secondary $PM_{2.5}$ mainly contributed to the long-range transport of $PM_{2.5}$ from the continent to the downwind area including the Sea of Japan and the East China Sea. In addition, eastward $PM_{2.5}$ fluxes averaged from the first to 10th layers along the line shown in Fig. 1 were calculated to examine the impacts of the direct effect on the long-range transport of $PM_{2.5}$. The mean contributions of the aerosol direct effect to the eastward fluxes of the total, primary and secondary $PM_{2.5}$ were about 1.5%, 0.1% and 2.5% decreases, respectively. These findings indicate that the decrease in the total amount of secondary $PM_{2.5}$ caused by the direct effect in the continent led to a smaller amount of $PM_{2.5}$ outflow to the downwind area.

Fig. 7 shows relationships of mean contribution percentage of the aerosol direct effect to the ground-level $PM_{2.5}$ concentration and shortwave radiation, and PBL height at each grid cell over the land area during the simulation period. The mean contribution of the aerosol direct effect to the $PM_{2.5}$ concentration showed clear negative correlations with that to both the shortwave radiation and PBL height (r = –0.86). These results indicate that, in land areas with substantial aerosol loading, the remarkable decrease of the downward shortwave radiation at the surface by the aerosol direct effect reduced the ground surface temperature and ground-level air temperature, and in turn, caused the reduction in PBL height, i.e., more stable lower atmosphere. As a result, suppressed vertical dispersion of air pollutants increased the ground-level $PM_{2.5}$ concentration.

Fig. 8 shows mean diurnal variations of the simulated surface shortwave radiation, PBL height and ground-level $PM_{2.5}$ concentration at Beijing and Osaka from January to March 2014. Compared to the one-way simulation, the mean daily maximum shortwave radiation at the ground surface in the two-way simulation was smaller by 155 W m^{-3} and 50 W m^{-3}, which are equivalent to 23% and 8.8%, at Beijing and Osaka, respectively. Similarly, the mean daily maximum PBL height was reduced by 414 m and 63 m, representing 33% and 4.8%, at Beijing and Osaka. The $PM_{2.5}$ concentration was clearly higher in the two-way simulation

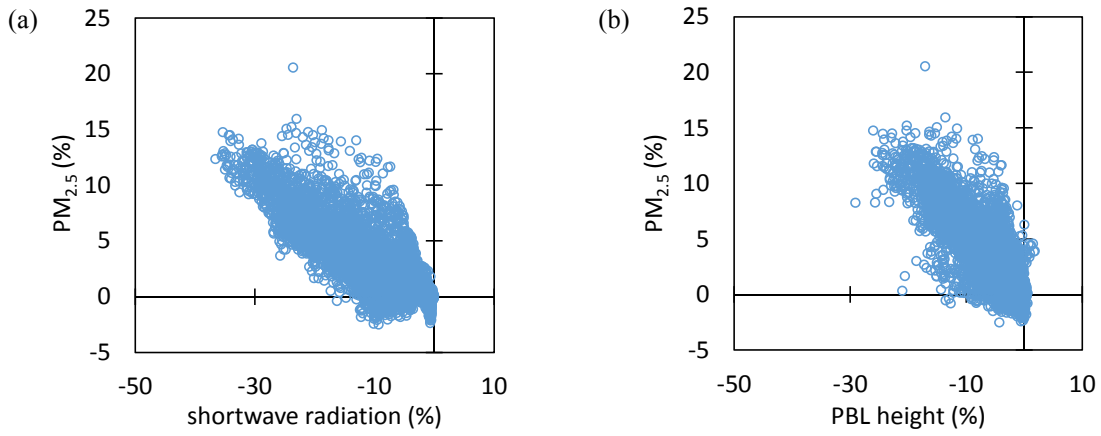

Fig. 7. Scatter plots of mean contribution percentage of the aerosol direct effect to ground-level $PM_{2.5}$ concentration and (a) surface shortwave radiation, and (b) PBL height for each grid cell in land areas.

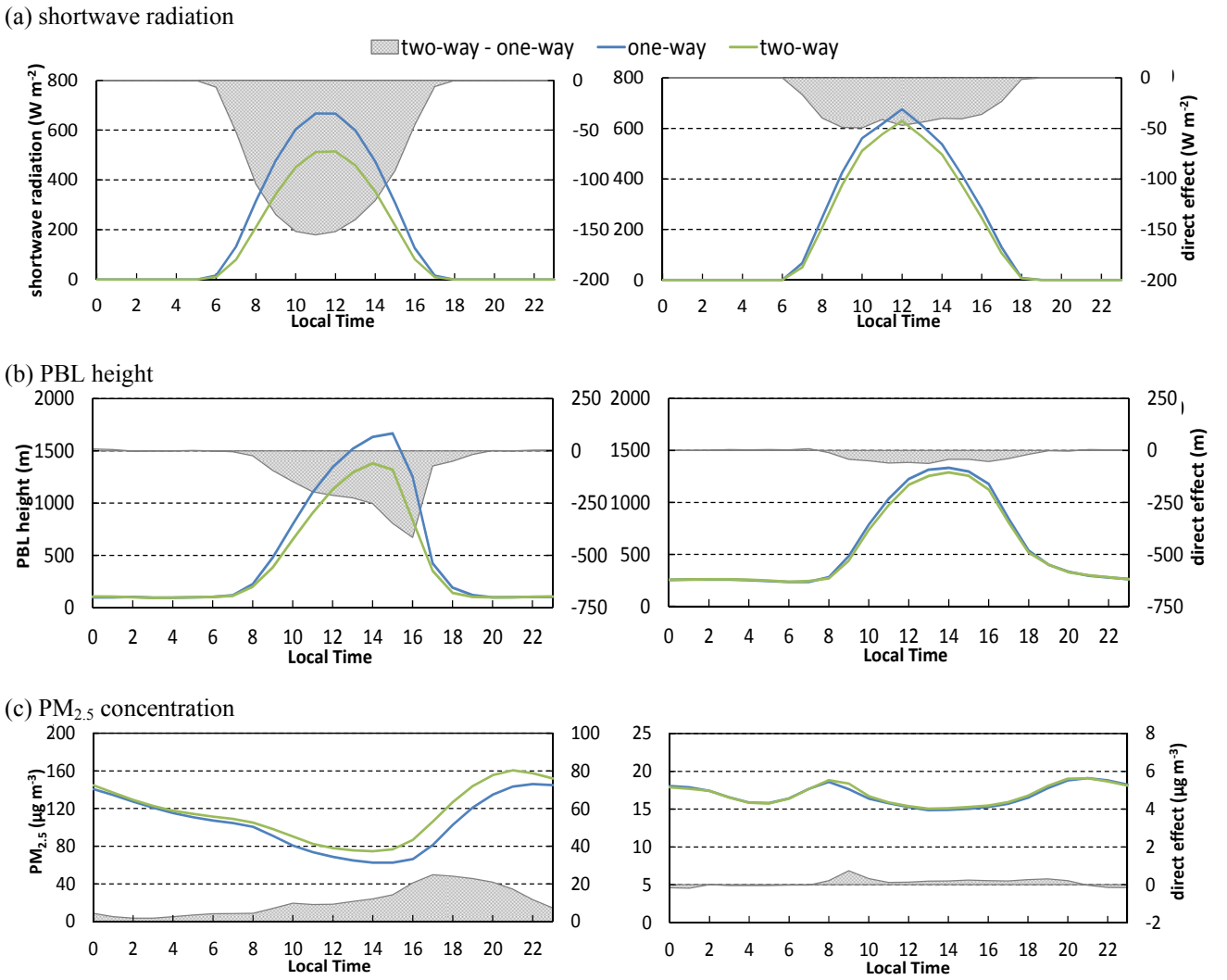

Fig. 8. Average diurnal variations of simulated (a) surface shortwave radiation, (b) PBL height and (c) ground–level $PM_{2.5}$ concentration at Beijing (in the left) and Osaka (in the right) from January to March 2014.

by up to 31% at Beijing, but the diurnal variation patterns in the one-way and the two-way simulations were almost similar at Osaka. In areas with heavy local $PM_{2.5}$ pollution, the aerosol direct effect decreased the surface shortwave radiation particularly around noon, the PBL height particularly in the afternoon. Although the PBL height during nighttime was quite similar in the two cases, the ground-level $PM_{2.5}$ that was locally accumulated during daytime under more stable atmospheric condition in the two-way simulation increased the concentration even in the evening.

CONCLUSIONS

The online coupled WRF-CMAQ modeling system was applied to one-way and two-way meteorological air-quality simulations of the winter from January till March of 2014 over East Asia. The two simulations were compared in order to quantify the impacts of the aerosol direct effect on the simulated meteorological and $PM_{2.5}$ fields in the study region with heavy local air pollution and long-range transport.

The comparison of the one-way and the two-way simulations showed that there were larger differences in the regions with high aerosol loading, particularly from Northeast to Central China. For the ground-level $PM_{2.5}$ concentration in Beijing, there was generally a positive contribution from the aerosol direct effect, especially on days with heavy air pollution. Meanwhile, for the $PM_{2.5}$ concentration in Osaka, which is strongly affected by long-range transport, a negative contribution from the direct effect occurred as frequently as a positive one. The aerosol direct effect decreased the surface shortwave by 15% and the PBL height by 9.0% on average over the regions from Northeast to Central China during the study period. On the other hand, while the aerosol direct effect generally increased the ground-level $PM_{2.5}$ concentration in these regions, with the mean increase being 8.6%, the effect decreased the $PM_{2.5}$ concentration over the ocean from the Sea of Japan to the East China Sea, with the mean decrease being 1.0%. There were clear inverse correlations between the negative contributions from the aerosol direct effect to the shortwave and PBL, and the positive contribution to the $PM_{2.5}$

concentration on the Asian continent. This finding indicates that the substantial decrease in the surface shortwave radiation due to the aerosol direct effect resulted in enhanced atmospheric stability, which favored the accumulation of ground-level $PM_{2.5}$. Moreover, the negative contribution from the direct effect to the ground-level $PM_{2.5}$ over the ocean was likely attributed to reduction in the secondary $PM_{2.5}$ outflow from the continent, which was caused by the increased dry deposition of $PM_{2.5}$ precursors because of the increased ground-level concentrations within a more stable PBL over the continent.

In summary, this study revealed that the aerosol direct effect influenced simulations of not only severe local pollution but also long-range transport of aerosol particles. Therefore, it is important to consider the aerosol direct effect in simulations of heavily polluted areas, which will lead to a better understanding of complicated interactions between the meteorology and the atmospheric chemistry in further studies. In addition, it should be noted that the influence of model settings, such as those related to emissions, boundary conditions, and grid nudging, on both model performance and the aerosol direct effect needs to be better quantified and understood. Finally, although this study focused on the aerosol direct effect, it is also important to apply an online coupled model with the aerosol indirect effect and evaluate the influences of full interactions between aerosols, radiation, and clouds on local pollution and long-range transport.

ACKNOWLEDGMENTS

This research was supported by JSPS KAKENHI Grant Number 26740038.

REFERENCES

Binkowski, F.S., Arunachalam, S., Adelman, Z. and Pinto, J.P. (2007). Examining photolysis rates with a prototype online photolysis module in CMAQ. *J. Appl. Meteorol. Clim.* 46: 1252–1256.

Byun, D.W. and Ching, J.K.S. (1999). Science algorithms of the EPA models-3 Community Multi-scale Air Quality (CMAQ) modeling system. NERL, Research Triangle Park, NC, U.S. Environmental Protection Agency publication EPA/600/R-99/030. U.S.

Chen, T.F., Chang, K.H. and Tsai, C.Y. (2014). Modeling direct and indirect effect of long range transport on atmospheric $PM_{2.5}$ levels. *Atmos. Environ.* 89: 1–9.

Cheng, Z., Luo, L., Wang, S., Wang, Y., Sharma, S., Shimadera, H., Wang, X. Bressi, M., de Miranda, R.M., Jiang, J., Zhou, W., Fajardo, O., Yan, N. and Hao J. (2016). Status and characteristics of ambient $PM_{2.5}$ pollution in global megacities. *Environ. Int.* 89–90: 212–221.

Diehl, T., Heil, A., Chin, M., Pan, X., Streets, D., Schultz, M. and Kinne, S. (2012). Anthropogenic, biomass burning, and volcanic emissions of black carbon, organic carbon, and SO_2 from 1980 to 2010 for hindcast model experiments. *Atmos. Chem. Phys. Discuss.* 12: 24895–24954.

Emery, C., Tai, E. and Yarwood, G. (2001). Enhanced meteorological modeling and performance evaluation for two Texas ozone episodes. Prepared for The Texas Natural Resource Conservation Commission 12118 Park 35 Circle Austin, Texas 78753.

Emmons, L.K., Walters, S., Hess, P.G., Lamarque, J.F., Pfister, G.G., Fillmore, D., Granier, C., Guenther, A., Kinnison, D., Laepple, T., Orlando, J., Tie, X., Tyndall, G., Wiedinmyer, C., Baughcum, S.L. and Kloster, S. (2010). Description and evaluation of the Model for Ozone and Related chemical Tracers, version 4 (MOZART-4). *Geosci. Model Dev.* 3: 43–67.

Fukui, T., Kokuryo, K, Baba, T. and Kannari, A. (2014). Updating EAGrid2000-Japan emissions inventory based on the recent emission trends. *J. Jpn. Soc. Atmos. Environ*. 49: 117–125. (in Japanese)

Guenther, A., Karl, T., Harley, P., Wiedinmyer, C., Palmer, P.I. and Geron, C. (2006). Estimates of global terrestrial isoprene emissions using MEGAN (Model of Emissions of Gases and Aerosols from Nature). *Atmos. Chem. Phys*. 6: 3181–3210.

Hogrefe, C., Pouliot, G., Wong, D., Torian, A., Roselle, S., Pleim, J. and Mathur, R. (2015). Annual application and evaluation of the online coupled WRF-CMAQ system over North America under AQMEII phase 2. *Atmos. Environ*. 115: 683–694.

Iacono, M.J., Delamere, J.S., Mlawer, E.J., Shephard, M.W., Clough, S.A. and Collins, W.D. (2008). Radiative forcing by long-lived greenhouse gases: Calculations with the AER radiative transfer models. *J. Geophys. Res*. 113: D13103.

Itahashi, S., Hayami, H., Uno, I., Pan, X. and Uematsu, M. (2016). Importance of coarse-mode nitrate produced via sea salt as atmospheric input to East Asian oceans. *Geophys. Res. Lett.* 43: 5483–5491.

Jiang, J., Zhou, W., Cheng, Z., Wang, S., He, K. and Hao, J. (2015). Particulate matter distributions in China during a winter period with frequent pollution episodes (January 2013). *Aerosol Air Qual. Res.* 15: 494–503.

JPEC (2012). Technical report of the Japan Auto-Oil Program: Emission inventory of road transport in Japan. JPEC Technical Report, JPEC-2011AQ-02-06. (in Japanese)

Kain, J.S. (2004). The Kain-Fritsch convective parameterization: An update. *J. Appl. Meteorol*. 43: 170–181.

Kong, X., Forkel, R., Sokhi, R.S., Suppan, P., Baklanov, A., Gauss, M., Brunner, D., Baro, R., Balzarini, A., Chemel, C., Curci, G., Guerrero, P.J., Hirtl, M., Honzak, L., Im, U., Perez, J.L., Pirovano, G., Jose, R.S., Schlünzen, K.H., Tsegas, G., Tuccella, P., Werhahn, J., Zabkar, R. and Galmarini, S. (2015). Analysis of meteorology-chemistry interactions during air pollution episodes using online coupled models within AQMEII phase-2. *Atmos. Environ*. 115: 527–540.

Kurokawa, J., Ohara, T., Morikawa, T., Hanayama, S., Janssens-Maenhout, G., Fukui, T., Kawashima, K. and Akimoto, H. (2013) Emissions of air pollutants and greenhouse gases over Asian regions during 2000-2008:

Regional Emission inventory in ASia (REAS) version 2. *Atmos. Chem. Phys.* 13: 11019–11058.

Morrison, H., Thompson, G. and Tatarskii, V. (2009). Impact of cloud microphysics on the development of trailing stratiform precipitation in a simulated squall line: Comparison of one- and two moment schemes. *Mon. Weather Rev.* 137: 991–1007.

Ohara, T., Akimoto, H., Kurokawa, J., Horii, N., Yamaji, K., Yan, X. and Hayasaka, T. (2007). An Asian emission inventory of anthropogenic emission sources for the period 1980-2020. *Atmos. Chem. Phys.* 7: 4419–4444.

OPRF (2012). Report for comprehensive study for environmental impact lead by the establishment of emission control area in Japan. Report ISBN978-4-88404-282-0. (in Japanese)

Pleim, J.E. (2006). A simple efficient solution of surface-profile relationships in the atmospheric surface layer. *J. Appl. Meteorol. Climatol*. 45: 341–347.

Pleim, J.E. (2007). A combined local and non-local closure model for the atmospheric boundary layer. Part 1: Model description and testing. *J. Appl. Meteorol. Climatol*. 46: 1383–1395.

Rienecker, M.M, Suarez, M.J., Todling, R., Bacmeister, J., Takacs, L., Liu, H.C., Gu, W., Sienkiewicz, M., Koster, R.D., Gelaro, R., Stajner, I. and Nielsen, J.E. (2008). The GEOS-5 data assimilation system: Documentation of versions 5.0.1, 5.1.0, and 5.2.0. NASA/TM-2008-104606, vol. 27. Technical Report Series on global modeling and data assimilation. Goddard Space Flight Center, Greenbelt, Maryland, 118 pp.

Shimadera, H., Hayami, H., Morino, Y., Ohara, T., Chatani, S., Hasegawa, S. and Kaneyasu, N. (2013). Analysis of summertime atmospheric transport of fine particulate matter in Northeast Asia. *Asia-Pac. J. Atmos. Sci.* 49: 347–360.

Shimadera, H., Hayami, H., Ohara, T., Morino, Y., Takami, A. and Irei, S. (2014). Numerical simulation of extreme air pollution by fine particulate matter in China in winter 2013. *Asian J. Atmos. Environ.* 8: 25–34.

Shimadera, H., Kojima, T. and Kondo, A. (2016). Evaluation of air quality model performance for simulating long-range transport and local pollution of $PM_{2.5}$ in Japan. *Adv. Meteorol*. 2016: 5694251.

Skamarock, W.C., Klemp, J.B., Dudhia, J., Gill, D.O., Baker, D.M., Duda, M.G., Huang, X.Y., Wang, W. and Powers, J.G. (2009). A description of the advanced research WRF version 3. NCAR Technical Note. NCAR/TN-475+STR.

Tan, J., Zhang, Y., Ma, W., Yu, Q., Wang, J. and Chen, L. (2015). Impact of spatial resolution on air quality simulation: A case study in a highly industrialized area in Shanghai, China. *Atmos. Pollut. Res*. 6: 322–333.

Uno, I., Sugimoto, N., Shimizu, A., Yumimoto, K., Hara, Y. and Wang, Z. (2014). Record heavy $PM_{2.5}$ air pollution over China in January 2013: Vertical and horizontal dimensions. *SOLA* 10: 136–140.

Wang, J., Wang, S., Jiang, J., Ding, A., Zheng, M., Zhao, B., Wong, D.C., Zhou, W., Zheng, G., Wang, L., Pleim, J.E. and Hao, J. (2014). Impact of aerosol-meteorology interactions on fine particle pollution during China's severe haze episode in January 2013. *Environ. Res. Lett.* 9: 094002.

Whitten, G.Z., Heo, G., Kimura, Y., McDonald, E.B., Allen, D.T., Carter, W.P.L. and Yarwood, G. (2010). A new condensed toluene mechanism for Carbon Bond: CB05-TU. *Atmos. Environ*. 44: 5346–5355.

Wiedinmyer, C., Akagi, S.K., Yokelson, R.J., Emmons, L.K., Al-Saadi, J.A., Orlando, J.J. and Soja, A.J. (2011). The Fire INventory from NCAR (FINN): A high resolution global model to estimate the emissions from open burning. *Geosci. Model Dev.* 4: 625–641.

Wong, D.C., Pleim, J., Mathur, R., Binkowski, F., Otte, T., Gilliam, R., Pouliot, G., Xiu, A., Young, J.O. and Kang, D. (2012). WRF-CMAQ two-way coupled system with aerosol feedback: Software development and preliminary results. *Geosci. Model Dev.* 5: 299–312.

Xing, J., Mathur, R., Pleim, J., Hogrefe, C., Gan, C.M., Wong, D.C., Wei, C. and Wang, J. (2015). Air pollution and climate response to aerosol direct radiative effects: A modeling study of decadal trends across the northern hemisphere. *J. Geophys. Res.* 120: 12221–12236.

Xiu, A. and Pleim, J.E. (2001). Development of a land surface model. Part I: Application in a mesoscale meteorological model. *J. Appl. Meteorol*. 40: 192–209.

Yan, R., Yu, S., Zhang, Q., Li, P., Wang, S., Chen, B. and Liu, W. (2015). A heavy haze episode in Beijing in February of 2014: Characteristics, origins and implications. *Atmos. Pollut. Res*. 6: 867–876.

Yu, S., Mathur, R., Pleim, J., Wong, D., Gilliam, R., Alapaty, K., Zhao, C. and Liu, X. (2014a). Aerosol indirect effect on the grid-scale clouds in the two-way coupled WRF-CMAQ: Model description, development, evaluation and regional analysis. *Atmos. Chem. Phys.* 14: 11247–11285.

Yu, S., Zhang, Q., Yan, R., Wang, S., Li, P., Chen, B., Liu, W. and Zhang, X. (2014b). Origin of air pollution during a weekly heavy haze episode in Hangzhou, China. *Environ. Chem. Lett.* 12: 543–550.

Zhang, Q., Streets, D.G., Carmichael, G.R., He, K., Huo, H., Kannari, A., Klimont, Z., Park, I., Reddy, S., Fu, J.S., Chen, D., Duan, L., Lei, Y., Wang, L. and Yao, Z. (2009). Asian emissions in 2006 for the NASA INTEX-B mission. *Atmos. Chem. Phys*. 9: 5131–5153.

Zheng, B., Zhang, Q., Zhang, Y., He, K.B., Wang, K., Zheng, G.J., Duan, F.K., Ma, Y.L. and Kimoto, T. (2015). Heterogeneous chemistry: A mechanism missing in current models to explain secondary inorganic aerosol formation during the January 2013 haze episode in North China. *Atmos. Chem. Phys*. 15: 2031–2049.

Received for review, June 30, 2016
Revised, November 7, 2017
Accepted, November 11, 2017